Solid Freeform Fabrication 2019: Proceedings of the 30th Annual International Solid Freeform Fabrication Symposium – An Additive Manufacturing Conference
Reviewed Paper

IN-PLANE PURE SHEAR DEFORMATION OF CELLULAR MATERIALS WITH NOVEL GRIP DESIGN

K. M. Conway[a], S. S. Kulkarni[a], B.A. Smith[a] G. J. Pataky[a], G. M. Mocko[a], J. D. Summers[a]

[a] Department of Mechanical Engineering, Clemson University, Clemson, SC 29634-0921, United States

Abstract

Cellular materials are popular due to their high specific strength, but their in-plane shear behavior is not well understood. Current experimental methods are limited due to the lack of pure shear loading as common arcan-style grips have not been adjusted for cellular materials. A significant concern is a mixture of shear loading with grip induced tension. While in bulk materials the tensile force can be assumed negligible, it has a significant impact on the deformation behavior of cellular materials. In this study, finite element modeling simulations were used to demonstrate that using a new sliding grip design reduced grip induced tension on cellular materials. Experimental studies were performed on honeycomb cellular materials with traditional and newly-developed grips to calculate and compare the shear strength and ductility of honeycomb cellular materials. The study concluded that traditional grips overestimate the shear strength of honeycomb cellular materials and honeycomb cellular materials in pure shear with limited grip induced tension has significantly lower strength and ductility due to the early formation of plastic hinges.

Introduction

Cellular materials are used in a variety of applications due to their ability to absorb energy [1,2], high specific strength [3,4] and controllable materials properties such as Poisson's ratio [4–6], toughness and yield strength [7]. To understand how cellular materials will deform in anticipated loading environments, the mechanical behavior of cellular materials under pure and mixed loads must be understood. The uniaxial tensile and compressive behaviors of cellular materials has been well documented [4,7–10]. Similar to foams, when cellular materials experience low velocity impacts, the material will experience shear loading [11]. However, the pure shear behavior of cellular materials has not been sufficiently studied experimentally, because most grip systems used in shear tests of cellular materials introduce a transverse constraint that adds a tensile component to the shear test [12–17]. Most experimental studies of shear in cellular materials use a three bar double shear test [12,15] or an offset grip single shear test [17], shown in Figure 1. Due to the nature of these grips, the width of the specimen is kept constant. This constraint in the horizontal direction adds a tensile component to the specimen, creating a combined shear and tension test, demonstrated in Figure 2. This combined loading artificially strengthens the specimen as the cellular material is stronger in tension then shear loading. In solid materials, this tensile component can be assumed negligible, however in cellular materials, due to the stress concentrations at beam intersections, small tensile loads will have a large impact on the shear failure strain of cellular materials [18].

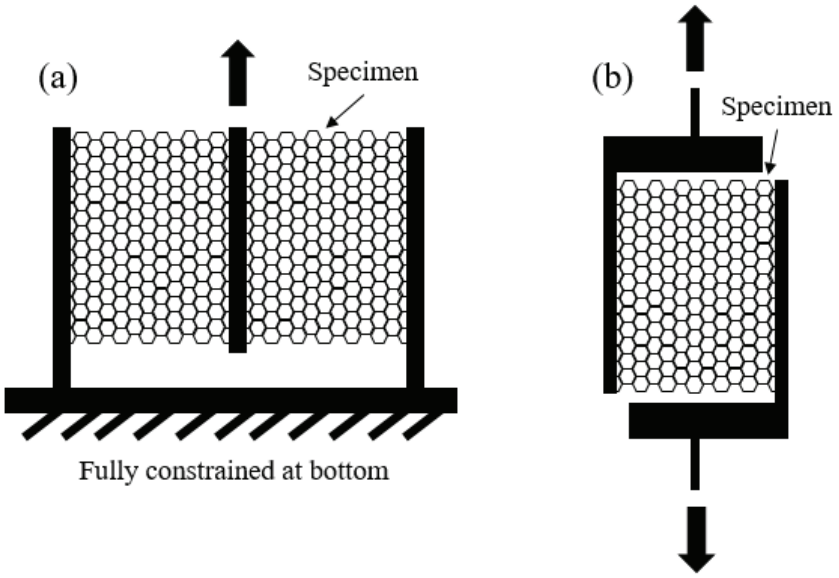

Figure 1: (a) Three bar double shear and (b) offset grip single shear test setups commonly used in shear tests for cellular materials introduces a horizontal constraint that adds a tensile load to test specimens.

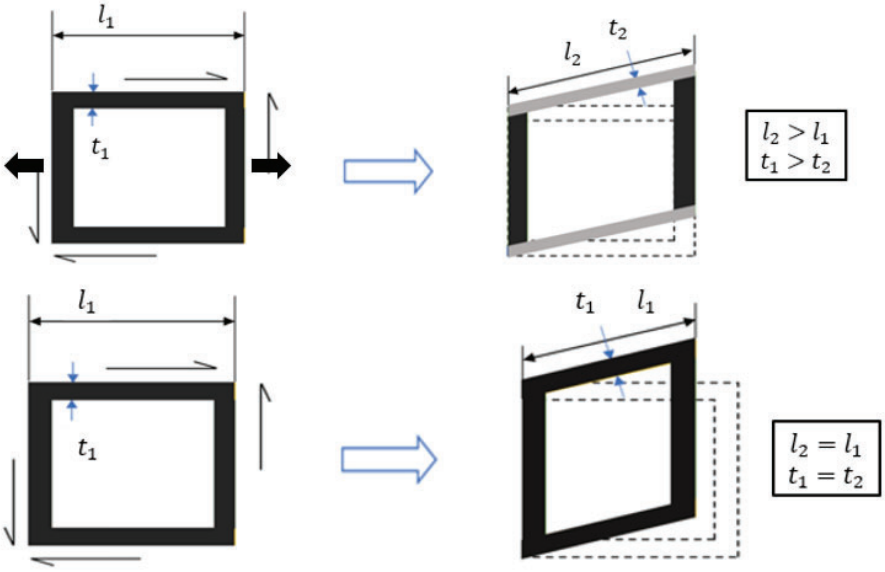

Figure 2: The difference in deformation of pure shear and combined shear and tension applied loads. The added tensile component in the combined shear and tension artificially strengthens materials stronger in tension.

While the limitations of current cellular material shear deformation grip designs has been discussed in literature [12,17], a grip design has not been adopted that is capable of true pure shear applied loads. Current experimental studies of cellular materials tested in pure shear continue to be combined loading, with the tensile component included [13,15]. Additionally, most numerical studies of shear loading of cellular materials also constrain the height of the specimen as to

maintain the same loading conditions of experimental studies [14–16,19]. Due to this, the magnitude of the effect the applied tensile load has on the cellular material cannot be quantified through a review of the literature.

In this study, traditional offset single shear grips and novel grips that do not constrain the transverse deformation of the cellular material were compared to quantify the effect of induced tension on the shear failure strain of cellular materials. A numerical modeling study of the honeycomb specimens in shear was used to model the differences in specimen behaviors in both loading scenarios and were compared with experimental results.

Methods and Materials

Honeycomb specimens were additively manufactured (AM) by fused deposition modeling (FDM) using AmazonBasic acrylonitrile butadiene styrene (ABS) white 1.75 kg spool filament in a Makerbot Replicator 2X. AM specimens were printed using a 0.4 mm nozzle, a nozzle temperature of 250 °C, a bed temperature of 110 °C, a layer height of 0.2 mm, and a print speed of 90 mm/s. The honeycomb shear specimens were ten cells tall and five complete cells wide with a wall thickness of 1.2 mm, a cell width of 4.35 mm and a total specimen thickness of 3.75 mm, producing a shear specimen with an effective area of 86.4 mm^2 using the method to calculate effect area discussed in [7]. After printing, the honeycomb specimens were polished with P120 grit sandpaper up to P1500 grit sandpaper.

Traditional offset single shear grips, referred to as the fixed-fixed grips in the study, were designed for the honeycomb shear specimens that kept the width of the specimen constant throughout testing, as can be seen in Figure 3a, inducing mixed loading on the specimens. Novel grips, referred to as the sliding-fixed grips (Figure 3b), were designed with a channel that allowed the grips to translate in the transverse direction during the test. A machinist at Clemson University manufactured both grips out of 316L stainless steel. A plastic shim with made of poly-lactic acid with an approximate coefficient of friction of 0.25 [20] was added to the channel of the sliding grips to minimize sliding resistance in the grip.

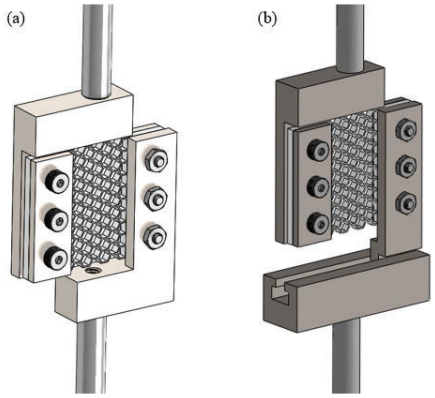

Figure 3: a) Offset single shear fixed-fixed grips. The width of the specimen is maintained throughout the shear test, inducing a tensile load on to the cellular material. b) Novel sliding-fixed grips that allow the grips to translate in during the test to eliminate the applied tensile load seen in the offset grips.

The grips were loaded in tension, thereby loading the cellular specimen in shear. The cellular shear specimens were tested to failure in two grip combinations: fixed-fixed and sliding-fixed. Experiments were performed as displacement-controlled at a displacement rate of 30 μm/s using an MTS Landmark 370 hydraulic load frame. A dual camera system was used for a multiscale understanding of the deformations. One camera was focused on the deformation of a single cellular unit cell while the other captured the global deformation of the entire specimen. Both cameras were Point Grey model GS3 and captured images at a rate of 1 Hz. Digital image correlation (DIC) was used to calculate the strains in the legs of the specimens during deformation. The camera capturing the deformation of a single unit cell was positioned directly in front of the specimen and was equipped with a Navitar lens and a Navitar 1X adaptor with a resolution of 120 pix/mm. The camera capturing the global deformation was positioned next to the first camera, slightly offset from the specimen and was equipped with a Schneider Kreuznach Xenoplan lens model 1001960. Images were used to calculate the full field displacements and strains using the commercial DIC software, VIC 2D. Strain calculations were performed with a virtual strain gage of 101 and a spatial resolution of 121 following the procedure outlined in [21]. Before testing, specimens were mechanically polished and speckled using an Iwata Custom Micro airbrush model CM-B2 and opaque black Testors Aztek airbrush paint, 9441A.

Numerical modeling simulated specimen loading scenarios using the finite element software ANSYS Workbench 17.0. Grips and specimens were modeled using Solidworks modeling software. The behavior of ABS is simulated using the Bergstrom-Boyce model to predict the non-linear viscoelastic response of the ABS elastomer. Tensile stress-strain data from FDM ABS was used to calibrate the material model. The material properties used in the simulation are summarized in Table 1. The geometries were meshed using the adaptive size function in Workbench, with coarse relevance center, medium smoothing and fast transition. The mesh settings result in a total of 6101 and 5925 solid elements (SOLID 186 & SOLID 187) for the fixed and sliding cases respectively. Specifically, the honeycomb structure is meshed using 5265 and 5323 quadratic tetrahedral Solid 187 elements (10 nodes), with three degrees of freedom, for the fixed and sliding cases respectively. The contact between the solid components is meshed using CONTA 174 and TARGE170 element pair. The boundary conditions used for modeling the two grips are summarized in Table 2. The system was modeled in tension, thus loading the cellular specimen in shear using a static structural analysis that did not consider strain rate dependent loading. Force displacement data from the experimental tests has been used to find the displacement value at which failure occurs. The distance is averaged over three test values.

To model both grips systems, appropriate boundary conditions were applied to mimic the conditions experienced by the physical grips. The fixed grip system was modeled by completely constraining the bottom grip, displacing the top grip in the vertical direction, and completely constraining rotation of the top plane of the grip. The bottom grip of the sliding system was also completely constrained, and the top grip displaced in the vertical direction, without rotation. However, a frictional contact (μ=0.3) was added to the system between the horizontal and vertical components of the grips to allow the grips to freely translate together and apart as the specimen is loaded. The boundary conditions can be seen in Figure 4.

Table 1: Material Properties used in simulation

Property	FDM ABS	316L Stainless Steel
Density [kg/m^3]	1050	7850
Young's Modulus [GPa]	1.54	200
Poisson's ratio	0.42	0.30
Bulk Modulus [GPa]	4.17	167
Shear Modulus [GPa]	8.93	76.29
Yield Strength [MPa]	29	250
Ultimate tensile strength [MPa]	30	460

Table 2: Boundary conditions used in simulation for fixed and sliding grips

Part	Fixed grips	Sliding grips
Upper bracket	Displacement (x=0, y=-6.8 mm, z=0)	Displacement (x=0, y=-6.3 mm, z=0)
Lower bracket	Fixed support	Fixed support
X axis separation	Constant	Frictional sliding with coefficient 0.3

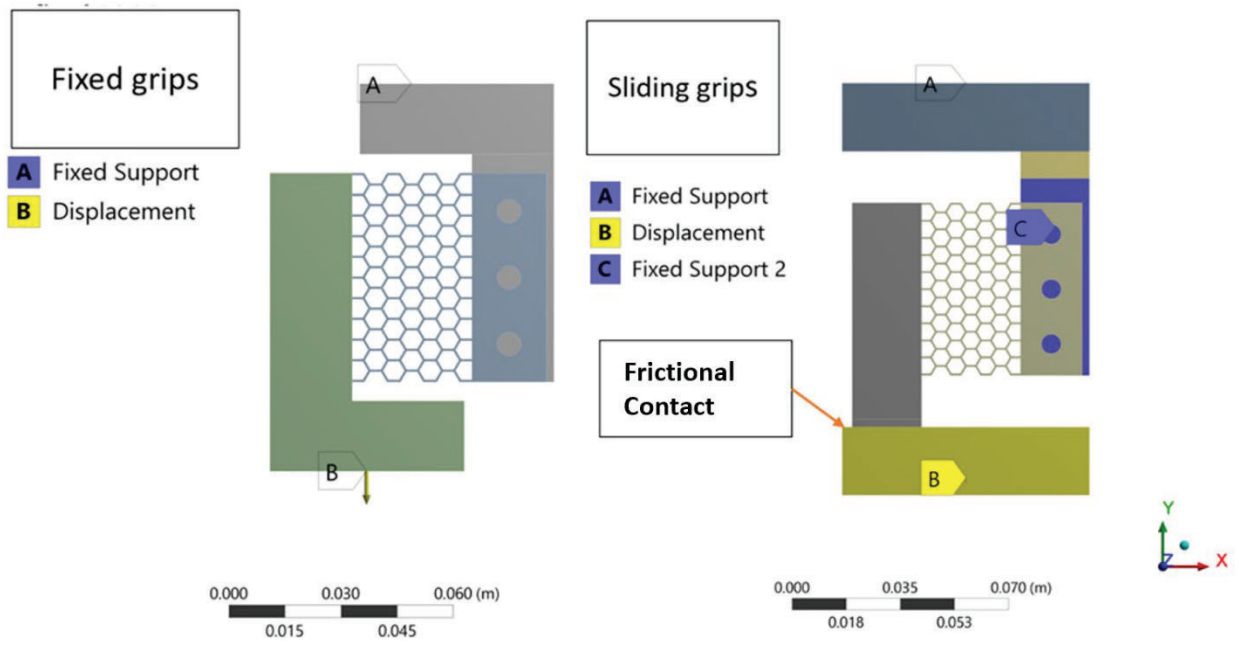

Figure 4: Boundary conditions of fixed and sliding grip systems in ANSYS model

Results and Discussion

Simulation of Both Grips

The deformation of honeycombs specimens in both the fixed and sliding grips were simulated to predict how local strains and forces would change between the grip systems. Table 3 shows the results for the fixed-fixed grips and the sliding-fixed grips. Comparing the strain values

between the sliding and fixed grips, the sliding grips exhibit an overall reduction in tensile strain with a maximum reduction of 23.08%. From this reduction in tensile strain in the sliding-fixed grips the simulation suggests that the fixed-fixed grips cause mixed loading on the specimen instead of pure shear and the sliding-fixed grips apply loading closer to pure shear.

Experimental Results of Fixed-Fixed Grips

Honeycomb specimens were tested to failure in the fixed-fixed grips. The specimens deformed in one of three manners. The first distinct way specimens failed was a uniform deformation of the entire specimen where all of the unit cells of the specimen would transform from hexagons to rotated rectangles as seen in Figure 5b. This uniform deformation is the deformation method captured by the simulation. During this deformation, plastic hinges formed at the intersections of the cell walls, as indicated by the large local shear strains shown in Figure 6.

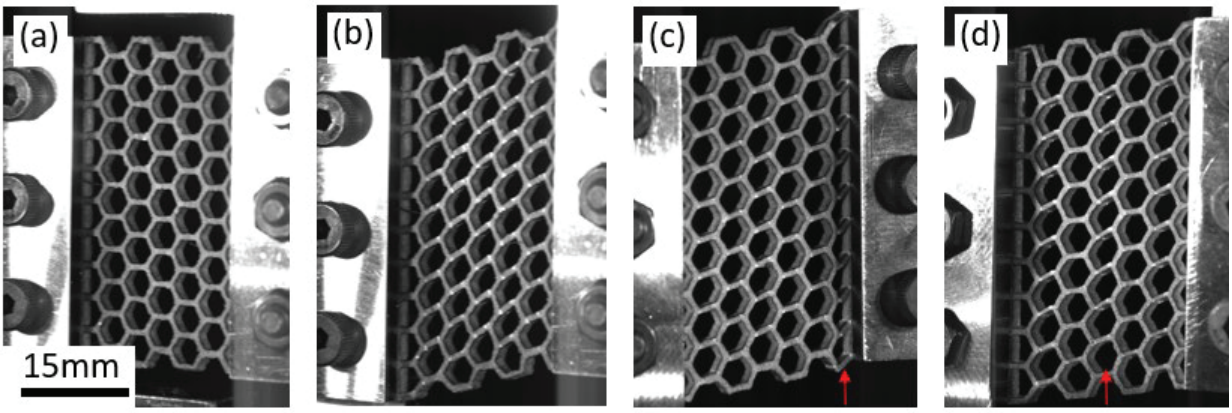

Figure 5: Honeycomb offset single shear specimen. Specimens failed in three distinct manners. a) Undeformed specimen. b) Uniform deformation: all hexagonal unit cells transform to rectangles with applied global shear loading. c) Deformation of cells at grip: Minor uniform deformation of hexagonal unit cells, horizontal cell wall grip fails, initiating immediate failure in entire column at wall. d) Major deformation in one column of cells in the specimen, other cells in specimen only experience minor deformation. ***Camera is offset, not square to specimen, to allow the camera capturing the close up unit cell deformation to be square. This is causing an optical illusion suggesting the specimen is deforming out of plane; it is not.***

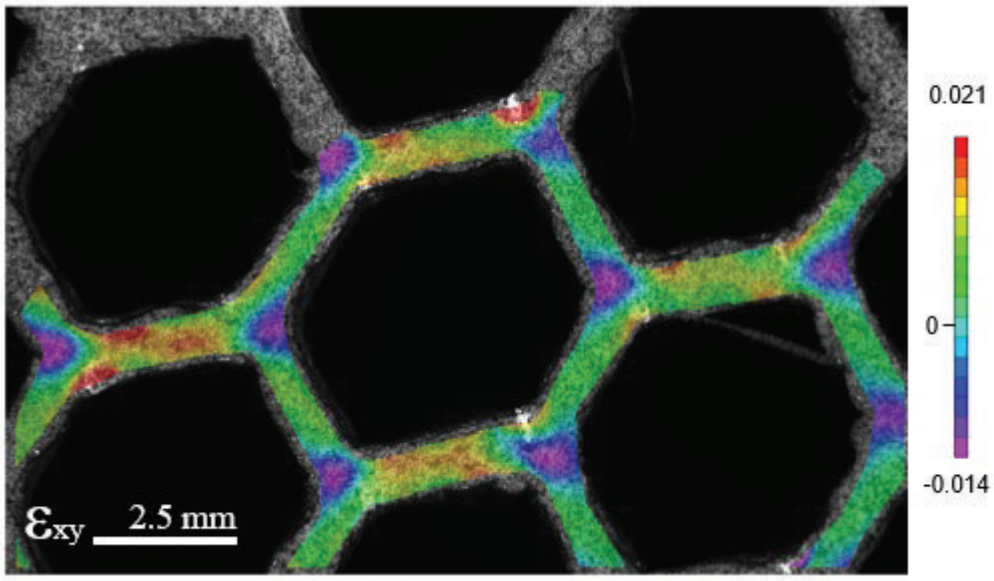

Figure 6: Plastic hinges formed at joints, as indicated by the large local shear strains, of the cellular material as the unit cells deformed from hexagons to rotated rectangles during global shear deformation

The second and third deformation modes involved the honeycomb failing at a single column. The specimen failed in a single column either at the wall of the specimen, Figure 5c, or at a column in the center of the specimen, Figure 5d. When the specimen failed at the column at the wall of the specimen, as seen in Figure 5c, the hexagonal unit cells did not deform to the degree seen in the uniform deformation case, Figure 5b. Instead the horizontal walls in the column attached to the specimen wall would develop plastic hinges and fail [18]. As often seen in cellular materials, when one wall or unit cell fails, the sudden increased loads on the neighboring cell walls leads to plastic collapse of the cellular material where the surrounding walls fail and the material fractures along a row of cells [9,10,15,18]. Similarly, this deformation method can occur in a column not adjacent to the specimen representing the third deformation method, as in Figure 5b. This occurs when one column deforms to a greater degree than its surrounding columns, so that the originally horizontal walls of the cells in the center column of the specimen rotate as the specimen is deformed, however the neighboring columns experience noticeably less deformation. The failure in one cell wall of the specimen that leads to the plastic collapse of the entire column is due to a stress concentration that causes the lack of integrity of that cell wall. In AM materials internal voids and printing defects will introduce stress concentrations throughout the build. These introduced stress concentrations during the build process explain the variation in the performance of the cellular specimens. Additionally noticeable crazing is present at the plastic hinges that develop as the cellular specimen deforms, further deforming areas with already pre-existing stress concentrations [22]. The variability in deformation modes between the specimens could be due to variation of defects from printing between the specimens. The surface of each specimen was polished to minimize the effects of surface flaws, however the inner wall of each honeycomb was not polished and surface flaws could have been present at the hinge points in the specimens. Flaws that are inherent in additively manufactured materials was not accounted for in the simulation

which accounts for why the honeycombs specimens in the fixed-fixed grips deformed one of three ways, but the simulation only deformed uniformly.

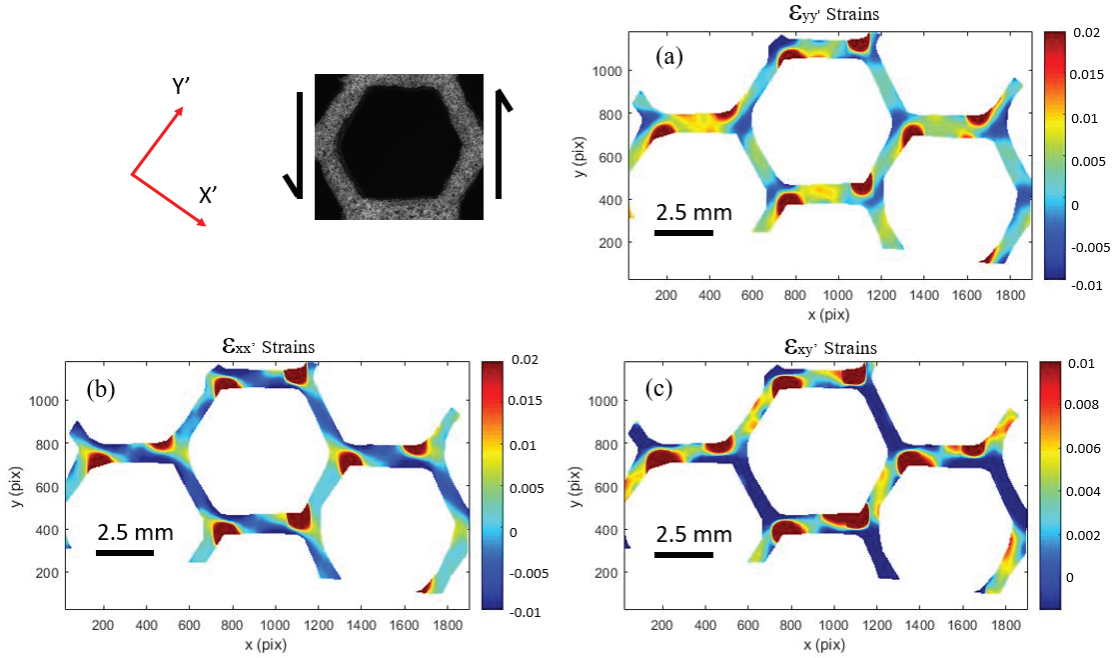

Figure 7: Strain transformations aligning with cell wall 30° CW off vertical of uniformly deformed offset single shear specimen

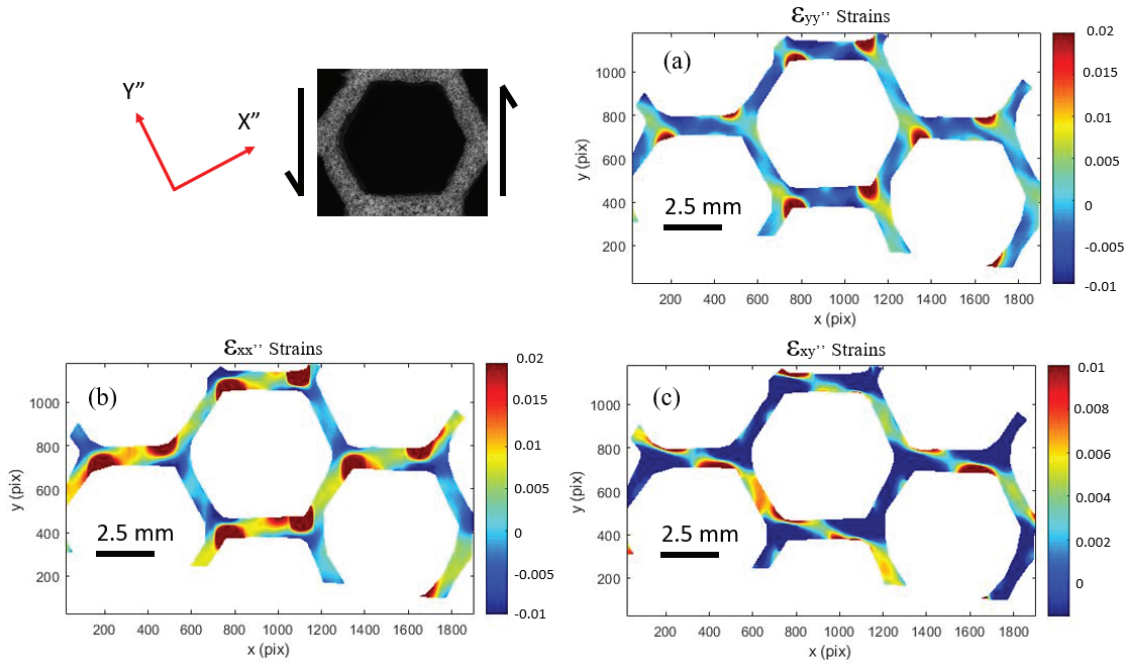

Figure 8: Strain transformations aligning with cell wall 30° CW off vertical of uniformly deformed offset single shear specimen

Strains calculated through DIC were rotated using the strain-transformation equations in Equations 1-3 to align with the angled cell walls of the honeycomb in the cellular specimen, Figure 9, using a MATLAB program. The rotated strains for the uniformly deformed specimen, Figure 5b, shown in Figure 7 and Figure 8. This allows for better understanding of the strains experienced by each cell wall.

$$\varepsilon_{x'} = \frac{\varepsilon_x + \varepsilon_y}{2} + \frac{\varepsilon_x - \varepsilon_y}{2} cos2\theta + \frac{\gamma_{xy}}{2} sin2\theta \quad (1)$$

$$\varepsilon_{y'} = \frac{\varepsilon_x + \varepsilon_y}{2} - \frac{\varepsilon_x - \varepsilon_y}{2} cos2\theta - \frac{\gamma_{xy}}{2} sin2\theta \quad (2)$$

$$\frac{\gamma_{x'y'}}{2} = -\frac{\varepsilon_x - \varepsilon_y}{2} sin2\theta + \frac{\gamma_{xy}}{2} cos2\theta \quad (3)$$

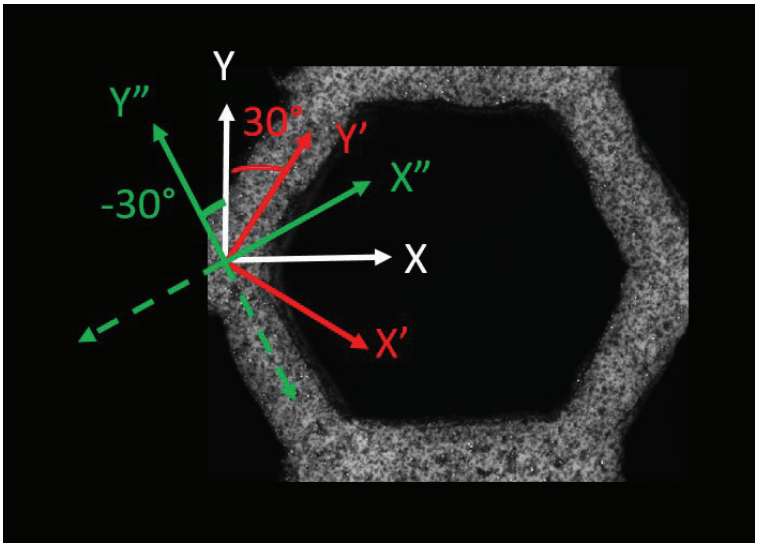

Figure 9: Strains calculated through DIC corresponding to the Y and X axis transformed to align with angled arms of honeycomb to the Y', X' and Y'', X'' axes

In the case where the cellular material deforms in a uniform manner, Figure 5b, as the honeycomb unit cells transitioned to rotated rectangles, all of the cell walls experience a positive tensile load. As the rotated rectangle is lengthened, the "long edges" of the rectangle are straightening due to the tensile component of the mixed load induced onto the cellular material by the grips. Additionally the cell walls that make up the "long edge" of the rectangle begin to bend to resist this deformation, as indicated by the large shear forces in the "long edge" walls in Figure 7c. As the honeycomb unit cell transitions to the rotated rectangle, a Poisson's effects of the rectangle narrowing causes the "short edge" of the rotated rectangle above and below to be loaded in tension as it resists this movement as indicated by the positive tensile loads in the "short edge" walls in Figure 8a. Additionally, plastic hinges form along with visible crazing at the triple junction in the middle of the "long edge" of the rectangle internal to the rectangle as the hinges are plastically deformed, resisting this deformation.

A comparison of the DIC results and the ANSYS model are shown in Figure 10. The model has good agreement with the DIC results for the magnitude and location of the local shear $\varepsilon_{xy}{}'$ strains, however the model disagrees with the DIC data on the location of the local $\varepsilon_{yy}{}'$ strains. This may be due to uneven deformation of the AM honeycomb specimen due to local flaws from the AM process which was unaccounted for in the simulation.

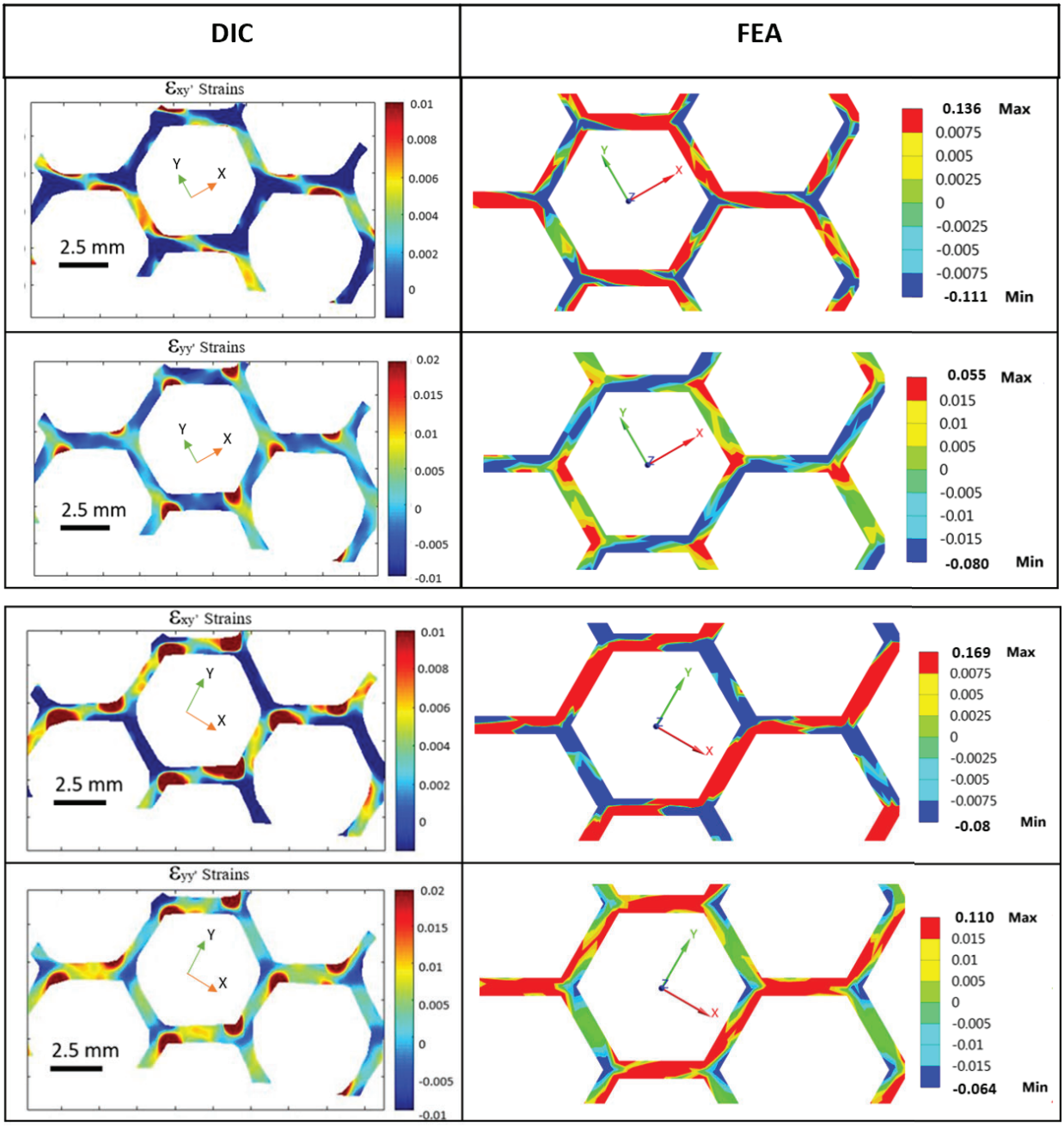

Figure 10: Comparison of DIC data of shear tests and ANSYS model of cellular material in shear in traditional grips with induced tension. The model has good agreement of the local $\varepsilon_{xy}{}'$ shear strains and fair agreement on the location of plastic hinges and concentration of $\varepsilon_{yy}{}'$ strains

The local shear strains of the fixed grips specimen show that the specimen is developing plastic hinges where two arms intersect as well as the arms of the specimen are bending. The formation of hinges is the dominate behavior, evidenced by the larger strains at the hinges as well as the eventual failure of the specimen at the hinges. As the specimen is loaded in shear, the transformation of the hexagonal honeycomb shape to rotated rectangles compresses the sides of the hexagon that form the long edge of the rectangle as well as the short end of the rectangle due to Poison's ratio as shown by the negative ε_{yy}' and ε_{yy}'' strains. Comparing the strain values, the ANSYS model predicted higher values of shear strain (ε_{xy}) and normal strain (ε_{yy}) when compared to the DIC data. This is attributed to the model not accounting for crazing in the ABS at the hinge locations where the specimen experiences the largest strains. Since the samples are additively manufactured, the material is non-homogeneous and anisotropic, while the simulation model assumes isotropic material, and does not account for crazing and plastic behavior. Due to this reason, the hinge effect is more pronounced in the case of DIC data. The simulation does not account for local defects which could result in non-uniform strain distribution in different hexagon wall locations, resulting in some cells with higher values of strains and some with lower.

Sliding-Fixed Shear Grips

When the honeycomb specimens were tested in the novel sliding grips, the specimen failed in a near pure shear deformation behavior, shown in Figure 11. The tensile component the sliding grips induced on the specimen was only due to sliding friction and was lower than the fixed grips. In the sliding-fixed grips, the center column of honeycomb cells failed in shear, however the surrounding cells did not transform into the rotated rectangles seen in the fixed grip specimens. A comparison of the final deformation appearance of the sliding grips and fixed grips is shown in Figure 12.

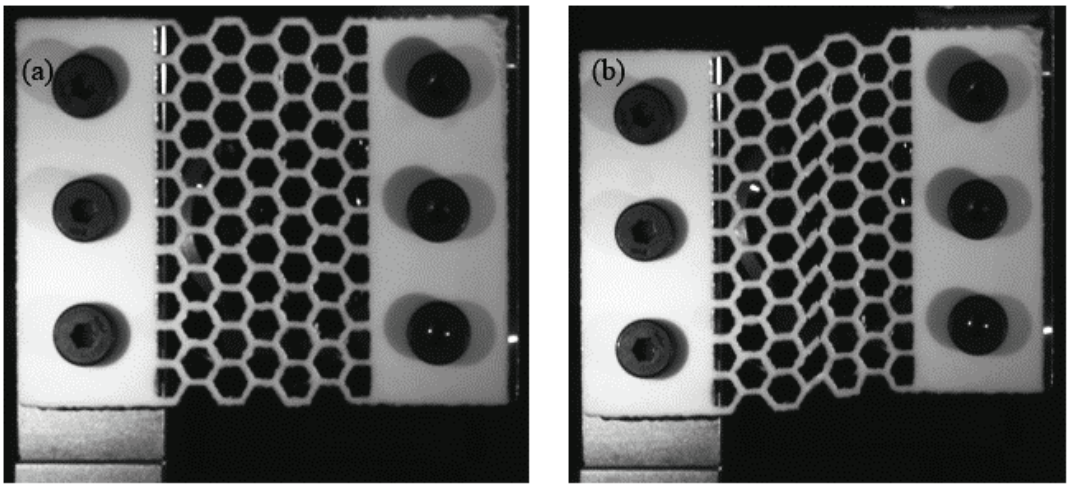

Figure 11: Shear deformation behavior of honeycomb specimen in new grips. (a) Specimen before loading (b) Specimen at maximum shear load, single row of cells failed in shear

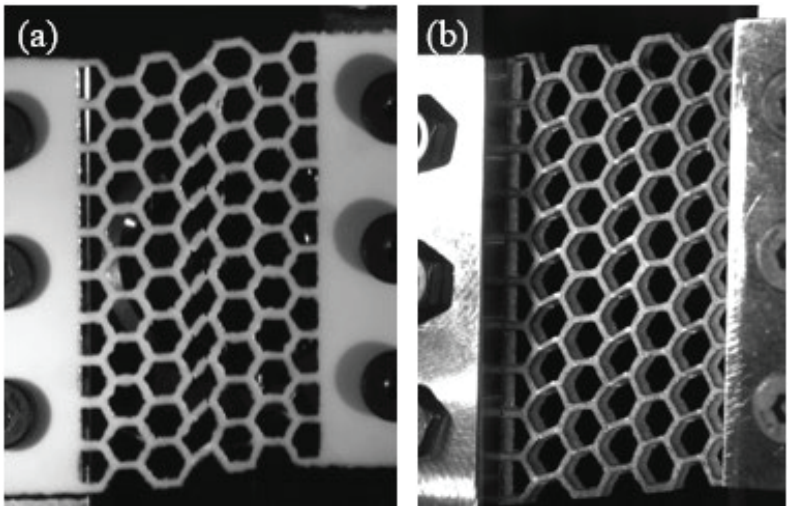

Figure 12: Comparison of deformation behavior of (a) sliding and (b) fixed grips. The fixed grips with grip-induced tension stretch cells between the grips forcing cells to transform into rotated rectangle geometries. Sliding grips do not stretch cells between grips causing the middle row to fail in a pure shear manner while neighboring cells do not transform.

The stress-strain response of the honeycomb specimens in the sliding grips are shown in Figure 13. The sliding grip specimens failed at a significantly lower stress and strain then the fixed grip specimens. This is because the honeycomb cellular specimens are stronger in tension then in pure shear. When the specimen deformed in the fixed grips, the grips cause the specimen to stretch between the grips. This causes all of the honeycomb cells to expand and transform into rotated rectangles. In the sliding grips, the honeycombs did not stretch between the grips and therefore not all of the joints in the honeycomb became plastic hinges, instead only the joints of the horizontal beam that sheared formed plastic hinges. The deformation caused very localized straining to occur on those few joints instead of distributing the strain throughout the entire transforming honeycomb as occurred on the fixed grip specimens. Mixed axial and shear loading causes the honeycomb specimen to fail at a yield strength approximately twice as large as pure shear loading and drastically increases the ultimate strain. Previous studies that have reported results as purely shear that were actually mixed shear and tension may have misreported the ultimate strength of the cellular material by half or more.

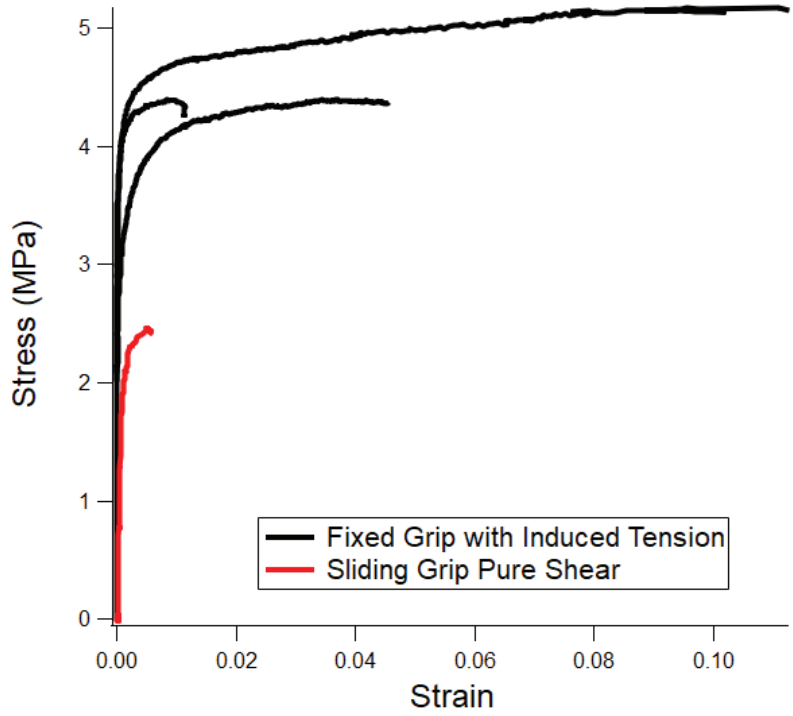

Figure 13: Stress-strain response of fixed and sliding grips. The fixed grips caused a combined loading of tension and shear on the honeycomb specimens. The combined loading artificially strengthened the honeycombs, as they are stronger in tension then in shear. The sliding grip tests illuminated that honeycomb cellular material is not as strong in shear as the fixed grip test results would otherwise indicate.

Local strains of the sliding grip honeycomb oriented with the angles axes of the honeycomb are shown in Figure 14. Plastic hinges form at the top left and bottom right of the horizontal beams. The high localization of strain in those few hinges leads to the early failure compared to the fixed grip specimens where the arms of the honeycomb experienced axial strains in addition to plastic hinging, Figure 7 and Figure 8. Deforming the honeycomb arms axially in the fixed grips as well as rotating the arms decreased the deformation experienced directly by the plastic hinges. Distributing the applied load throughout the honeycomb specimen in the induced tension grips allowed the honeycomb specimen to reach a higher ultimate strength as well as a larger ultimate global strain before failure due to the deformation of all or many of the honeycomb unit cells.

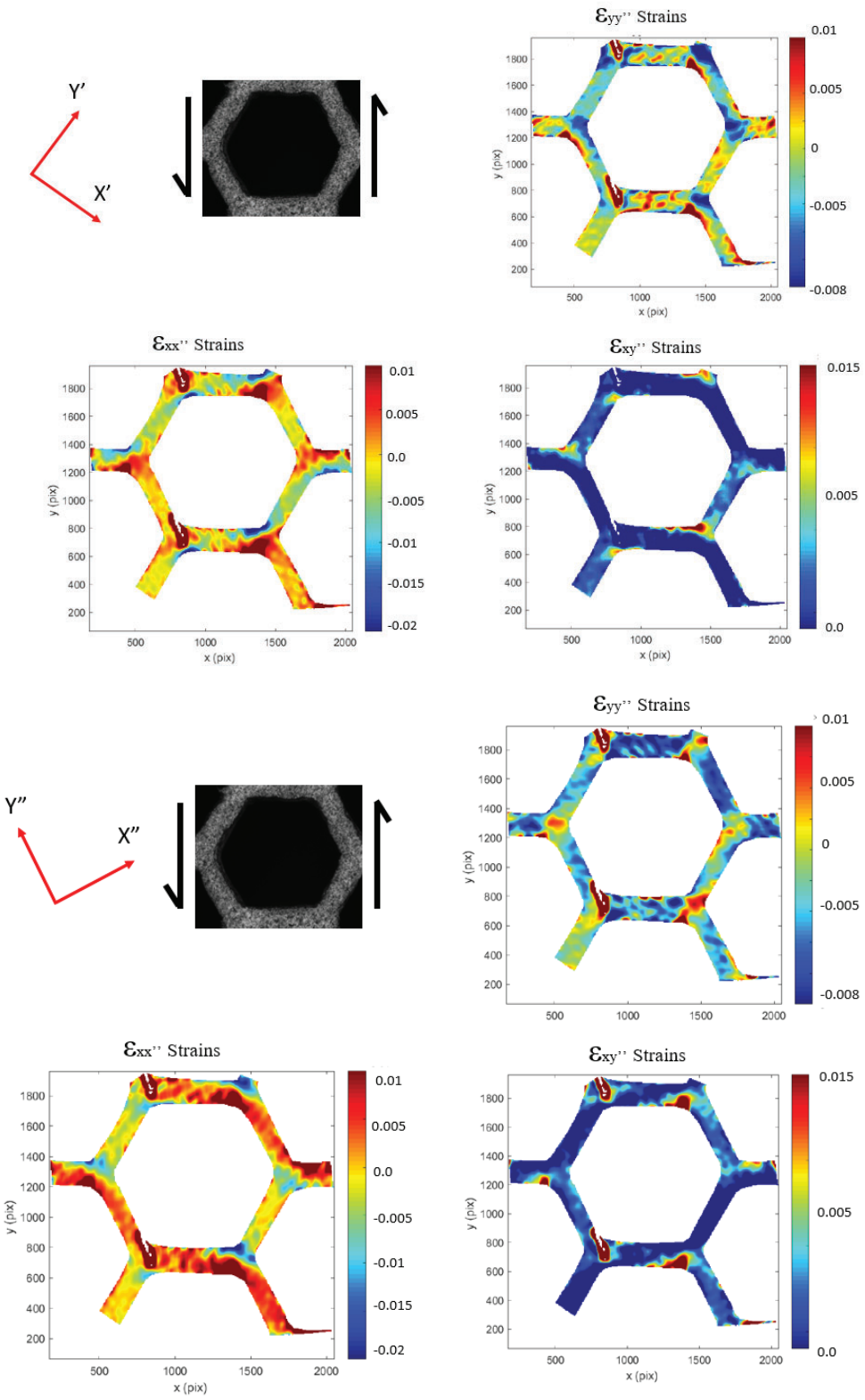

Figure 14: Local strains of the sliding grips oriented with the angled axes of the honeycombs. Plastic hinges, indicated by high local strains, formed at the top left and bottom right of the horizontal beam, the location where the beam will ultimately fail

The simulations of the sliding grips showed good agreement with the DIC as far as the location of the plastic hinges in the sliding grips as shown in Figure 15. The simulation however did not agree on the magnitude of the strains of the sliding grips. As with the fixed grips, this disagreement in magnitude is probably due to the simulation not considering crazing of the ABS honeycombs at the hinges. By not considering crazing, a toughening mechanism in ABS, the simulation over predicts the magnitude of the strains at the hinges as the honeycomb deforms.

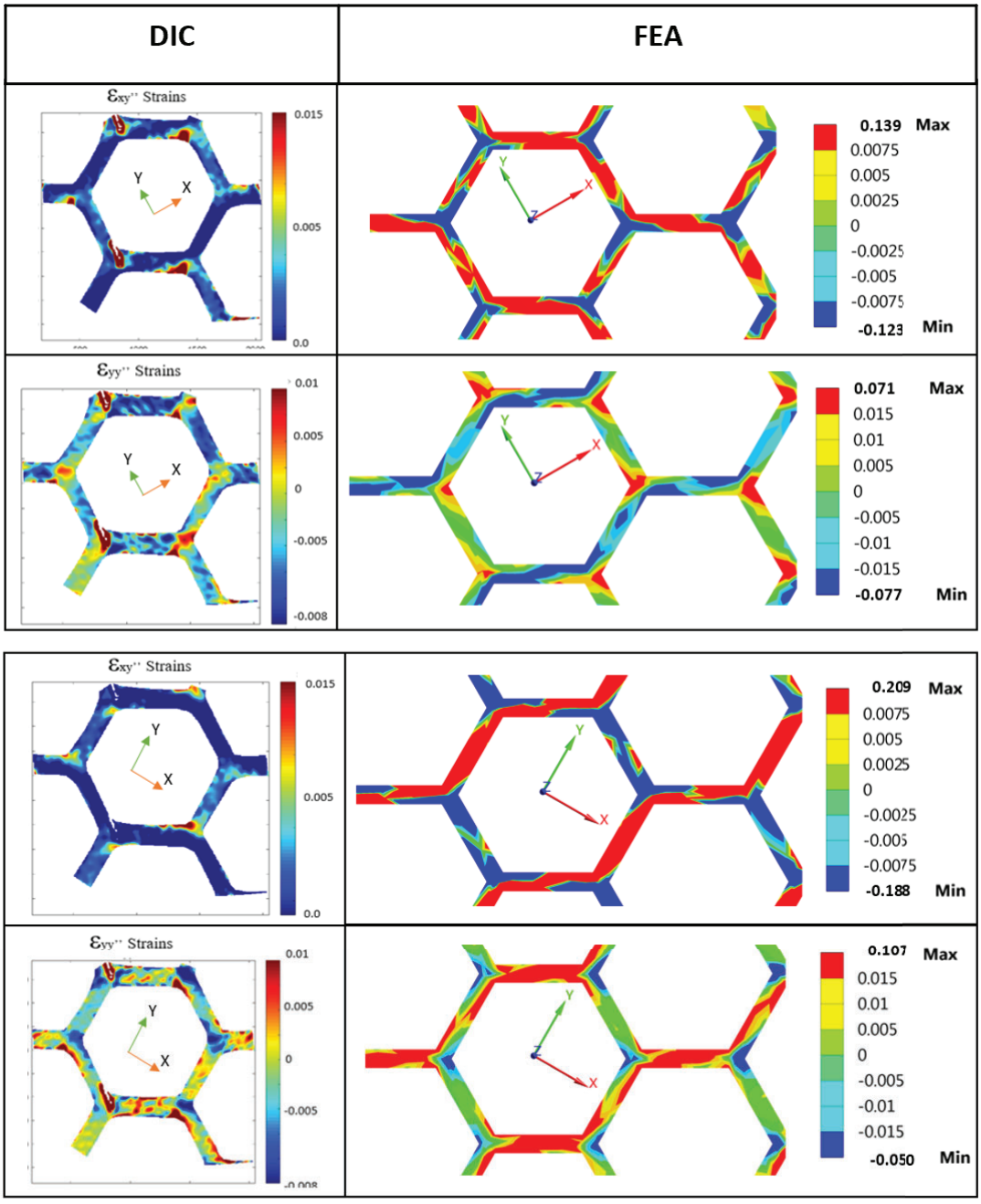

Figure 15: Good agreement of the local strain locations and magnitudes between local strain predictions of simulations of the honeycomb specimen in sliding grips and DIC results. The finite element model predicts a reduction in induced tension strain and an increase in the shear strain

when using the sliding grips (Table 4), demonstrating the differences in the loading effects on the specimens of the two grip designs.

Table 3. Comparison of tensile and shear strains (maximum value) between grips for simulation

Grip type	Coordinate system	Strain value	Simulation	$\left(\frac{\varepsilon_{sliding} - \varepsilon_{fixed}}{\varepsilon_{sliding}}\right) \times 100$
Fixed grips	30 degrees anticlockwise	ε_{yy}	0.08	
		ε_{xy}	0.136	
	30 degrees clockwise	ε_{yy}	0.110	
		ε_{xy}	0.169	
Sliding grips	30 degrees anticlockwise	ε_{yy}	0.077	-3.75%
		ε_{xy}	0.139	2.21%
	30 degrees clockwise	ε_{yy}	0.107	-2.72%
		ε_{xy}	0.209	23.67%

The simulation was correctly able to predict the location of plastic hinges and local strain concentrations on the honeycomb specimens for both grips. Due to this, finite element analysis could be used for future studies to determine the effect of mixed axial and shear loading on other topologies and determine which topologies require experimental study to determine the effect of mixed axial and shear loading and which geometries can be determined through simulation.

Conclusion

Traditional cellular material shear tests add a tensile component to the cellular materials. While previously assumed negligible, this study showed that the added tensile force artificially strengthened honeycomb cellular materials. Honeycomb cellular materials are stronger in combined tension-shear then pure shear. Under combined loading the entire honeycomb cell transformed to a rotated rectangle, distributing the strain throughout all of the honeycomb cells. In pure shear loading, the only part of the cell that deformed was plastic hinges on either side of the horizontal arm of the honeycomb and only the cells in a single column developed plastic hinges, not allowing the strain to be distributed the rest of the cells. Honeycomb cellular material in combined loading is about twice as strong as honeycombs in pure shear, showing that previous studies may have over reported the strength of honeycomb cellular materials in shear.

Acknowledgements

The authors would like to acknowledge experimental facilities provided by the Center for Integrated Nanotechnologies (CINT). Sandia National Laboratories is a multimission laboratory managed and operated by National Technology & Engineering Solutions of Sandia, LLC, a wholly owned subsidiary of Honeywell International Inc., for the U.S. Department of Energy's National Nuclear Security Administration under contract DE-NA0003525. This paper describes objective technical results and analysis. Any subjective views or opinions that might be expressed in the paper do not necessarily represent the views of the U.S. Department of Energy or the United States Government.

References

[1] Y.Y. Tay, C.S. Lim, H.M. Lankarani, A finite element analysis of high-energy absorption cellular materials in enhancing passive safety of road vehicles in side-impact accidents, Int. J. Crashworthiness. 19 (2014) 288–300. doi:10.1080/13588265.2014.893789.

[2] J. Schultz, D. Griese, J. Ju, P. Shankar, J.D. Summers, L. Thompson, Design of Honeycomb Meso-Structures for Crushing Energy Absorption, J. Mech. Des. 134 (2012) 071004. doi:10.1115/1.4006739.

[3] X.J. Ren, V. V. Silberschmidt, Numerical modeling of low density cellular materials, Comput. Mater. Sci. 43 (2008) 65–74.

[4] J. Lee, J.B. Choi, K. Choi, Application of homogenization FEM analysis to regular and re-entrant honeycomb structures, J. Mater. Sci. 31 (1996) 4105–4110. doi:10.1007/BF00352675.

[5] Y. Sun, N.M. Pugno, In plane stiffness of multifunctional hierarchical honeycombs with negative Poisson ' s ratio sub-structures, Compos. Struct. 106 (2013) 681–689. doi:10.1016/j.compstruct.2013.05.008.

[6] P. Shankar, J. Ju, J.D. Summers, J.C. Ziegert, Design of Sinusoidal Auxetic Structures for High Shear Flexure, in: Int. Des. Eng. Tech. Conf. Comput. Inf. Eng. Conf., ASME, Montreal, Canada, Canada, 2010: pp. DETC2010-28545.

[7] K.M. Conway, G.J. Pataky, Effective area method for calculating global properties of cellular materials, Mater. Today Commun. 17 (2018) 144–152. doi:10.1016/j.mtcomm.2018.09.003.

[8] D. Restrepo, N.D. Mankame, P.D. Zavattieri, Programmable materials based on periodic cellular solids. Part 1: Experiments, Int. J. Solids Struct. 100 (2016) 485–504. doi:10.1016/j.ijsolstr.2016.09.021.

[9] S.D. Papka, S. Kyriakides, Experiments and full-scale numerical simulations of in-plane crushing of a honeycomb, Acta Mater. 46 (1998) 2765–2776. doi:10.1016/S1359-6454(97)00453-9.

[10] F. Brenne, T. Niendorf, H.J. Maier, Additively manufactured cellular structures: Impact of microstructure and local strains on the monotonic cyclic behavior under uniaxial and bending load, J. Matierals Process. Technol. 213 (2013) 1558–1564.

[11] J. Zhou, Z.W. Guan, W.J. Cantwell, The Impact Response of Graded Foam Sandwich Structure, Compos. Struct. (2013) 370–377.

[12] Q. Zhou, R.R. Mayer, Characterization of Aluminum Honeycomb Material Failure in Large Deformation Compression, Shear, and Tearing, J. Eng. Mater. Technol. 124 (2002) 412. doi:10.1115/1.1491575.

[13] A.-J. Wang, D.L. McDowell, In-plane stiffness and yield strength of periodic metal honeycombs, J. Eng. Mater. Technol. 126 (2004) 137. doi:10.1115/1.1646165.

[14] Z.J. Kolla A, Ju J, Summers J, Fadel G, A. Kolla, J. Ju, J.D. Summers, G.M. Fadel, J.

Ziegert, Design of Chiral Honeycomb Meso-Structures for High Shear Flexure, in: Int. Des. Eng. Tech. Conf. Comput. Inf. Eng. Conf., ASME, Montreal, Canada, Quebec, Canada, 2010: pp. DETC2010-28557. doi:10.1115/DETC2010-28557.

[15] D. Pasini, Theoretical and Experimental Characterization of the 34.6 2D Lattice Material, Eng. Conf. 28158 (2010) 1–10.

[16] J. Ju, J.D. Summers, Compliant hexagonal periodic lattice structures having both high shear strength and high shear strain, Mater. Des. 32 (2011) 512–524. doi:10.1016/j.matdes.2010.08.029.

[17] S. Joshi, J. Ju, L. Berglind, R. Rusly, J.D. Summers, J.D. DesJardins, Experimental Damage Characterization of Hexagonal Honeycombs Subjected to In-Plane Shear Loading, in: ASME Int. Des. Eng. Tech. Conf. Comput. Inf. Eng. Conf., ASME, 2010: pp. 35–41. doi:10.1115/DETC2010-28549.

[18] L.J. Gibson, M.F. Ashby, Cellular Solids, structures and properties, 2nd ed., Cambridge University Press, Cambridge, 1997. doi:10.1016/S0304-0208(08)72856-1.

[19] J. Ju, B. Ananthasayanam, J.D. Summers, P. Joseph, Design of cellular shear bands of a non-pneumatic tire -investigation of contact pressure, SAE Int. J. Passeng. Cars - Mech. Syst. 3 (2010). doi:10.4271/2010-01-0768.

[20] P.K. Bajpai, I. Singh, J. Madaan, Tribological behavior of natural fiber reinforced PLA composites.pdf, Wear. 297 (2013) 829–840.

[21] P. Reu, Virtual strain gage size study, Exp. Tech. 39 (2015) 1–3. doi:10.1111/ext.12172.

[22] K.M. Conway, G.J. Pataky, Crazing in additively manufactured acrylonitrile butadiene styrene, Eng. Fract. Mech. 211 (2019) 114–124. doi:10.1016/j.engfracmech.2019.02.020.